

LFP Power Spectra in V1 Cortex: The Graded Effect of Stimulus Contrast

J. Andrew Henrie and Robert Shapley

Center for Neural Science, New York University, New York, New York

Submitted 3 September 2004; accepted in final form 7 February 2005

Henrie, J. Andrew and Robert Shapley. LFP power spectra in V1 cortex: the graded effect of stimulus contrast. *J Neurophysiol* 94: 479–490, 2005. First published February 9, 2005; doi:10.1152/jn.00919.2004. We recorded local field potentials (LFPs) and single-unit activity simultaneously in the macaque primary visual cortex (V1) and studied their responses to drifting sinusoidal gratings that were chosen to be “optimal” for the single units. Over all stimulus conditions, the LFP spectra have much greater power in the low-frequency band (≤ 10 Hz) than higher frequencies and can be described as “1/f.” Analysis of the total power limited to the low, gamma (25–90 Hz), or broad (8–240 Hz) frequency bands of the LFP as a function of stimulus contrast indicates that the LFP power gradually increases with stimulus strength across a wide band in a manner roughly comparable to the increase in the simultaneously recorded spike activity. However, the low-frequency band power remains approximately constant across all stimulus contrasts. More specifically the gamma-band LFP power increases differentially more with respect to baseline than either higher or lower bands as stimulus contrast increases. At the highest stimulus contrasts, we report as others have previously, that the power spectrum of the LFP typically contains an obvious peak in the gamma-frequency band. The gamma-band peak emerges from the overall broadband enhancement in LFP power at stimulus contrasts where most single units’ responses have begun to saturate. The temporal/spectral structures of the LFP located in the gamma band—which become most evident at the highest contrasts—provide additional constraints on potential mechanisms underlying the stimulus response properties of spiking neurons in V1.

INTRODUCTION

Ensemble activity of groups of neurons and how ensemble activity relates to single-unit activity are likely to be important clues to understanding the function of cortical circuitry (Buzsaki 2004). For instance, the mechanism underlying orientation selectivity of single-unit responses in V1 remains controversial even after over 40 yr of studying single neurons (Ferster and Miller 2000; Hubel and Wiesel 1962; Shapley et al. 2003). Competing models of V1 orientation selectivity, which can account for single-unit discharge properties, can be distinguished by the tuning properties of the underlying synaptic activity (both excitation and inhibition) (cf. for review Shapley et al. 2003). In a more generic context, when a stimulus-related change in the firing rate of an individual neuron is observed in V1, there remains some ambiguity as to the underlying cause due to the established functional significance of both synaptic excitation and inhibition (Borg-Graham et al. 1998; Hirsch et al. 1998). An increase in firing rate could be caused by an increase in excitation or a decrease in inhibition,

or an increase in both, or a decrease in both. A first step at disambiguating some of the biophysics underlying the single-unit properties could be to consider the overall level of synaptic activity. The local field potential (LFP) provides an easily obtainable measure of the activity in a local population—an ensemble—of neurons (Pesaran et al. 2002), which can be compared with spike activity measured simultaneously at the same site.

The LFP is defined as the low-frequency (below ~ 250 Hz) components of the raw field potential. These low-frequency fluctuations are thought to be dominated by current flow due to synaptic activity, whereas the higher-frequency components (> 300 Hz) are probably dominated by the currents associated with neuron action potentials (Destexhe 1998; Freeman 2000; Logothetis 2002; Nicholson and Freeman 1975; Mitzdorf 1985). Due to the conductive properties of the gray matter, the sources of the LFP are thought to be located within ~ 500 μm (Kruse and Eckhorn 1996). Thus the LFP-recording electrode notionally samples the activity of a population containing perhaps thousands of neurons (Kruse and Eckhorn 1996; Logothetis 2002; Mitzdorf 1985; Pesaran et al. 2002). The aggregate neural activity across an ensemble of neurons is captured by the LFP indirectly through synaptic activity. The link between the LFP and population activity through synaptic activity is corroborated by the observation that fluctuations in the LFP are highly correlated with simultaneously measured intracellular voltage fluctuations (McCormick et al. 2003; Penttonen et al. 1998; Steriade et al. 1996) that are synaptically driven.

A previous study of the LFP in V1 has shown that the total LFP power increased with stimulus contrast in a gradual manner very roughly comparable to spike activity and the functional magnetic resonance imaging (fMRI) signal (Logothetis et al. 2001). However, it was not clear from Logothetis et al. (2001) if the LFP power was particularly concentrated in the gamma frequency band at all contrasts or only at the higher contrasts. Furthermore, other previous studies involving the LFP in V1 have specifically assessed orientation selectivity and found that the gamma-band power was differentially more modulated by stimulus orientation than other frequency bands (Frien et al. 2000; Siegel and Konig 2003). Others have simply shown that the gamma-band limited power was modulated by stimulus orientation and peaked for angles near the peak for spike activity (e.g., Gray and Singer 1989). From the previous work, it remains unclear whether the gamma-band peak in the response spectrum is present for all stimulus conditions, with an overall scaling of the response magnitude, or if the spectral

Address for reprint requests and other correspondence: J. A. Henrie, Center for Neural Science, New York University, 4 Washington Place, Rm 809, New York, NY 10003 (E-mail: jah@cns.nyu.edu).

The costs of publication of this article were defrayed in part by the payment of page charges. The article must therefore be hereby marked “advertisement” in accordance with 18 U.S.C. Section 1734 solely to indicate this fact.

contents of the LFP are actually modulated by stimulus conditions.

We studied the neural activity recorded in V1 of anesthetized and paralyzed monkeys to a series of grating patterns of ascending stimulus contrasts. The simultaneously sampled LFP and spike responses from these recordings were analyzed to clarify the conditions under which gamma-band components of the LFP specifically distinguish themselves from the other LFP components as well as to explore what information the LFP can lend to our understanding of the spike responses when they are both recorded within the same paradigm by which previous work in single-unit physiology has elucidated the workings of V1 cortex (Shapley et al. 2003). Most single neurons in V1 are sensitive along a variety of stimulus dimensions, including: orientation, spatial frequency, temporal frequency, size, position, contrast, and color. For a single unit in V1, a stimulus value along these dimensions can be found that produces a maximum steady-state firing rate by measuring tuning curve along each dimension. We define such a stimulus as "optimal." Spike trains recorded under these conditions are indistinguishable from random (e.g., Poisson) processes (Holt et al. 1996; Shadlen and Newsome 1998; Softky and Koch 1993). Hence in this paradigm neural responses are typically quantified by the average number of spikes elicited in a time window of the order of seconds.

The biggest difference between this study and previous studies of the LFP in V1 is our use of stimuli that are optimal in size for single units. These optimal stimuli typically subtend 0.5–1.0° of visual angle in monkey (Sceniak et al. 2001) because of the prevalence of strong "surround suppression" in V1. Elongated or larger visual stimuli usually produce much smaller responses in V1 neurons than optimal stimuli. Previous studies of the LFP in V1 have used relatively large (>5°) or full field gratings. (e.g., Frien et al. 2000; Gail et al. 2004; Logothetis et al. 2001) Thus the LFP responses in V1 have been measured under conditions very much outside of the paradigm with which most single-unit responses have been investigated. (Indeed, the somewhat controversial reports of single- and multi-unit responses in V1 where temporal structure has been found also have also been studied outside of the optimal stimulus paradigm (e.g., Friedman-Hill et al. 2000).

Our main results are that the contrast dependence of the LFP is different in different frequency bands and that the LFP power spectrum changes shape with contrast with a peak in the gamma band (25–90 Hz) emerging at high contrast. We observed that the power spectra of the LFP have much greater power in the low-frequency band (e.g., ≤10 Hz) than at higher frequencies. Analysis of the contrast dependences of the frequency bands of the LFP spectrum indicates that the LFP power across a broad frequency band gradually increases with stimulus contrast. The largest increase in LFP power is seen specifically in the gamma frequency band. Therefore at the highest stimulus contrasts, the power spectrum of the LFP typically contains an obvious peak in the gamma frequency band, whereas the simultaneously observed spike trains contain little if any detectable structure in the corresponding frequency range. However, despite the largely unstructured spike responses, at the highest contrasts, there is a differential increase in the coherence between the LFP and spikes specific to the gamma band. Changes in the spectral content of the LFP with visual stimulation constitute, via Fourier's theorem, a change

in the temporal structure of the LFP. The most prominent change we observe is in the increase in the gamma-band activity that emerges in the LFP at high contrast. The increase of this particular temporal structure evident in the aggregate activity across an ensemble, but not apparently in individual spike trains, is consistent with the predictions of V1 models in which feed-forward inputs are nonlinearly amplified by recurrent circuitry that is dominated by inhibition (Tao et al. 2004a). Moreover, the gradual increase in the strength of the gamma-band activity within the ensemble as the overall level of feed-forward input and/or overall level of activity in the network increases is a generic feature of networks involving recurrent excitation and inhibition (Brunel and Wang 2003; C. Geisler, N. Brunel, and X. J. Wang, unpublished data).

METHODS

Animal preparation

Acute experiments were performed on 11 adult Old World monkeys (*Macaca fascicularis*) weighing between 1.5 and 3 kg in strict compliance with National Institutes of Health and institutional guidelines for the care and experimental use of animals. The methods of preparation and single-cell recording are essentially the same as those described previously (Hawken et al. 1996; Ringach et al. 1997; Xing et al. 2004). Anesthesia was induced with ketamine (5–20 mg/kg im), and venous cannulation and tracheotomy were carried out under isoflurane (1.5–3.5% in air). Throughout the remainder of the experiment anesthesia was maintained with sufentanyl (sufentanyl citrate, 6 $\mu\text{g} \cdot \text{kg}^{-1} \cdot \text{h}^{-1}$ iv). Muscle paralysis was induced and maintained with pancuronium or vecuronium bromide (Pavulon/Norcuron, 0.1 mg $\cdot \text{kg}^{-1} \cdot \text{h}^{-1}$ iv). A broad spectrum antibiotic (Bicillin, 50,000 IU/kg im) and antiinflammatory steroid (dexamethasone, 0.5 mg/kg im) were administered daily during the recording period. Electrocardiogram (EKG), electroencephalogram (EEG), and end-tidal CO_2 were continuously monitored, and blood pressure was measured noninvasively at 5-min intervals. Body temperature was maintained at 37°C.

EEG leads were attached to the skull above the frontal bone, differentially amplified, and monitored continuously on an oscilloscope. Anesthesia was controlled such that the EEG was consistent with light sleep (Steriade et al. 1996).

Experiments were terminated by intravenous injection of a lethal dose of pentobarbital after which the animal was quickly perfused through the heart with fixative (1.25% paraformaldehyde, 2.5% glutaraldehyde in phosphate buffer, pH 7.4). After perfusion, blocks of the occipital lobe containing the electrode tracks were removed and saved for histological reconstruction of the electrode track as described in Hawken et al. (1988, 1996)

Optics

Both pupils were dilated with topical administration of 1% atropine sulfate and immediately protected with gas permeable contact lenses. After surgery, the eyes were stabilized with ophthalmic rings (Duckworth and Kent, UK) to prevent drift of visual field position and treated with topical antibiotic (Gentamicin sulfate, 3%) as well as an ophthalmic antiinflammatory agent, Tobradex (.3% Tobramycin and 0.1% Dexamethazone mixture). External lenses were used to correctly focus the display monitor image on the retina. This correction was initially estimated with an ophthalmoscope and later improved by optimizing the responsiveness of spike activity for high spatial frequency stimulation. Both foveas were mapped using a reversible ophthalmoscope onto a tangent screen, where receptive fields could also be mapped in relation to the foveal position.

Electronics/data acquisition

The electrode was advanced through the gray matter with a micro-drive step motor (Narashige). Electrodes were glass-coated tungsten with exposed tips of 5–15 μm (Merrill and Ainsworth 1972) and $\sim 1\text{--}10\text{ M}\Omega$ impedance (measured at 1 kHz). Electrode signals passed through a headstage amplifier (100 \times), further amplified with a Dagan 2400 extracellular preamplifier (500 \times), which was sent to a Dagan EX4-400 differential amplifier where the signal was split to two signals. The first signal was AC coupled at 0.3–3 Hz (high-pass at 10 kHz) and sent to a CED 1401plus A/D box controlled by Spike2 (CED, Cambridge, UK) software. This box also recorded the timing syncs from the stimulus CRT. These data were digitized at a sampling rate of 10 or 20 kHz. The other signal was AC coupled with a low-frequency cutoff of 300 Hz and fed into the audio inputs of SGI workstation (O2 or Octane2, SGI) where single units were discriminated in custom software (D. L. Ringach) on the basis of the spike amplitude and waveform. The times of spike onset and the stimulus sync TTL were recorded to 0.01-ms resolution. These spike and sync times were then sent to an on-line experiment control and analysis program running on a separate computer Windows XP computer. This program (OPEQ, P. E. Williams and J. A. Henrie) consists of a graphical user interface (GUI) to the data running in Matlab 6.5.

Stimulus generation

Stimuli were generated on custom software (OPEQ) written in C using standard OpenGL graphics routines and running in Linux with an nVidia graphics card having OpenGL optimization. Data collection was synchronized with the screen refresh to a precision of <0.01 ms. The screen (Sony GDM-F520 Trinitron Color Graphic Display) measured 40.38 cm wide and 30.22 cm high with $1,024 \times 768$ pixels, running at 100.0-Hz frame refresh. The mean luminance (L_{mean}) of the screen was measured to be 98cd/m² at mean gray with a spectroradiometer, and the range from minimum (black) to maximum (white) stimulus intensities was carefully linearized in luminance through a look-up table. The screen viewing distance was 115 cm.

Visual stimulation was performed monocularly through the dominant eye. The nondominant eye was occluded. The stimulus contrast for all the drifting sine wave gratings that were used as stimuli was measured in units of Rayleigh contrast

$$c = (L_{\text{max}} - L_{\text{min}}) / (2 \cdot L_{\text{mean}}) \quad (1)$$

All gratings were windowed with a circular aperture beyond which the surrounding screen was set to the mean gray level equal to the mean luminance of the contrast defined grating (i.e., $c = 0$, $L_{\text{mean}} = 98\text{cd/m}^2$ outside the aperture). In a series of experiments, the values of several key stimulus parameters (orientation, spatial frequency, temporal frequency, and stimulus size) were chosen to maximize the discharge rate (or 1st harmonic amplitude, for simple cells) of the single unit under study. The typical sequence of experiments performed to find the optimal stimulus parameters was orientation, spatial frequency, temporal frequency, then size. The experiments that measure how the response scales with stimulus contrast were typically performed before the size experiments, but the size was usually close to optimal and all other stimulus parameters were optimal for the contrast experiments.

Data processing

The raw data collected with the Spike2 software were written to binary files using CED's native scripting language, and all subsequent analyses were performed in Matlab 6.5. Due to appreciable line noise (60 Hz) in the raw data, the following de-noising procedure was used. The magnitude and phase of the 60-Hz line noise was estimated on overlapping 4-s blocks of raw data using multiple regression over five Slepian data tapers (Mitra and Pesaran 1999; Thomson 1982). Then

for every data sample the amplitude and phase of the line noise was calculated by interpolation, and the line noise's Fourier component was synthesized and finally subtracted from the raw signal. This procedure slightly overestimates the line noise amplitude, hence in some spectra a slight notch at 60 Hz is evident in some power spectra. A different de-noising procedure that underestimated the line noise amplitude (hence a slight bump in the spectra) does not change any of the general results discussed here. The LFP was extracted from the raw signals by application of finite impulse response (FIR) digital filters using standard Matlab functions. The resulting pass band due to the electronic AC coupling and digital low-pass filtration was roughly 2.5–250 Hz.

Spectral analysis

The LFP is related to the level of ensemble activity through fluctuations in intracellular voltage. For this reason, quantifying the LFP activity is done by computing the power spectrum. The power spectrum is a measure of the variance in the signal as a function of frequency and is related to the time domain signal through the Fourier transform of the auto-correlation function.

LFP spectrograms were computed on $T = 500$ -ms windows, every $\Delta T = 50$ ms from time series sub-sampled to 500 Hz. We used the multi-taper method of Thomson (82, 90) (Mitra and Pesaran 1999; Pesaran et al. 2002; Thomson and Chave 1991), which provides a principled trade-off between minimizing the variance of the estimate and maximizing the spectro-temporal resolution. The application of tapers to the data allows for an estimate of power robust against bias that is particularly important for time series with a large dynamic range (Percival and Walden 1993). The particular choice of tapers used here—a family of orthogonal tapers, given by the prolate spheroidal functions (a.k.a. Slepian functions)—are parameterized by their length in time, T , and their bandwidth in frequency, W . The first $k = 2TW - 1$ of these Slepian data tapers are suitably concentrated in frequency for spectral estimation and, due to their orthogonality, result in independent estimates of power spectral density (PSD). Hence, for the $T = 500$ -ms windows of data used here, a bandwidth of $W = 4$ Hz was attained by using three Slepian data tapers. For each 500-ms time series, the mean was subtracted and then the signal was multiplied by each of the three orthogonal Slepian tapers. The Fourier components were then computed via FFT, and the PSD (denoted S), was derived by taking square of the modulus of these complex numbers corresponding to frequencies from 0 (DC) to 250 Hz (Nyquist frequency).

Although the time evolution of the LFP is interesting and dynamic in a way contrasting with spike dynamics (data not presented, but cf. Logothetis et al. (2001)), only the steady-state average behavior is considered here. Thus each LFP record for a given stimulus condition was summarized by a single spectrum by averaging across trials, tapers, and time. This produced $N = N_{\text{tapers}} \cdot N_{\text{trials}} \cdot N_{\text{times}}$ spectral estimates. Because of redundancy in the estimates created by using highly overlapping data segments, the degrees of freedom of the estimate are reduced. An overlap factor, $\xi = \Delta T/T$, was applied yielding $N_{\text{indep}} = N \cdot \xi$ as an approximate number of independent spectral estimates. A robust estimate of the spectrum and its confidence limits was performed via a bootstrapping procedure (Efron and Tibshirani 1986) similar to the jackknife suggested by Thomson and Chave (1991). Briefly, repeated (bootstrapped) means, $\langle S \rangle$, over N_{indep} samples drawn (with replacement) from all the estimates were made, yielding a distribution of $\langle S \rangle$. These distributions were empirically very close to the theoretical χ^2 distributions (Percival and Walden 1993) and were symmetrized by taking a log transform. The 99% confidence intervals of the spectra were then calculated assuming a t -distribution with $N_{\text{indep}} - 1$ df on the $\ln(\langle S \rangle)$ distribution.

Each raw spectrum could be characterized as “red” or “1/f,” and often had a local maximum somewhere between 25 and 90 Hz (gamma band) that was obvious even amid the large-scale structure of

the spectrum. Following Pesaran et al. (2002), we designated the frequency band 25–90 Hz as the gamma band. Although the gamma-band spectral structure was apparent in the raw spectra, normalization was necessary to compare the results between penetrations. Due to variation in the electrical characteristics of the electrodes between different penetrations and variation in the settings of the amplifiers, the units of the continuous records are arbitrary. Therefore the units of the spectra are also arbitrary. Indeed, although the spectrum of the LFP during baseline (no stimulus) was generally $1/f$ for all recordings, the exact shape was variable from penetration to penetration. To compare spectra from site to site across many penetrations and animals, the spectra were normalized in the following way. The mean of the power for each frequency was estimated over all “blank” or “baseline” conditions (bl) from a given experimental recording, yielding S_{bl} , as described in the preceding text. Using these quantities we calculated the modulation with respect to baseline, R . Thus all spectra, S , from a single experimental record were transformed to a quantity R by

$$R(f) = S(f)/S_{bl}(f) \quad (2)$$

which produces “modulation” spectra amenable to comparison from site to site. For plotting purposes, this can be expressed as a percentage change from baseline by

$$\Delta R(f) = 100\% \cdot R - 100\% \quad (3)$$

Again, 99% confidence intervals of the R (and ΔR) spectra were estimated via a boot-strapped t -statistic.

Normalizing the power, frequency by frequency, by either the baseline mean (e.g., Juergens et al. 1999; Siegel and Konig 2003) as we did here or by the standard deviation (SD) (e.g., Kayser et al. 2003; Logothetis et al. 2001) yields nearly identical results.

Spectral analysis of spikes was done analogous to the LFP analysis but with five Slepian tapers ($W = 6$ Hz). On each $T = 500$ -ms segment, the spike trains were histogrammed at 1-ms resolution, and the total number of spikes was subtracted, yielding a zero mean time series. More tapers were necessary to produce robust spectral estimates for the spike trains compared with the LFP due to the reduced signal to noise of the estimate due to discrete sampling (Jarvis and Mitra 2001; Pesaran et al. 2002). The spike-spectra were normalized by the Poisson expectation at the high-frequency limit (i.e., the average firing rate estimated over the same analysis window) (Jarvis and Mitra 2001) to more simply address the spectral content of the spike trains. Likewise, the spike-LFP coherence was estimated using seven Slepian data tapers ($W = 8$ Hz). The coherence is the magnitude of the complex valued coherency and provides a measure of the linear correlation between the spikes and LFP in the frequency domain (Mitra and Pesaran 1999; Pesaran et al. 2002). For visualization purposes, all spectra were smoothed in frequency with a Gaussian filter of the appropriate bandwidth, W .

Contrast response functions

Spike activity was quantified by either the mean spike rate (or F1 harmonic component for “simple” cells). Responses recorded during at least three repeats of gratings drifting for 1–4 s each at 12 different contrasts (2, 3, 4, 6, 8, 13, 17, 23, 33, 47, 68, and 96%) were used to estimate the mean response at each recording site for optimal stimulation. The baseline (0% contrast) level was also estimated from blank periods interspersed between stimulation periods where no stimulus contrast was present on the computer screen. This blank time also minimized fatigue and adaptation effects associated with long-term stimulation. Contrast response functions were derived for band-limited LFP activation by integrating the estimated spectrum corresponding to each stimulus contrast across a range of frequencies. Three bands were defined. First, the “low” (<10 Hz)-frequency band captures the bulk of total LFP power. The “broad” (8–240 Hz)-frequency

band corresponds well with the RMS measurement of LFP activity previously correlated with stimulus contrast by Logothetis et al. (2001). Finally, the “gamma” (25–90 Hz) band has been somewhat arbitrarily defined but is consistent with typically reported ranges (cf. Siegel and Konig 2003), and the actual range has negligible effect on the results presented here. The frequency band around the stimulus refresh rate [100 ± 4 (SD) Hz, where $W = 4$ Hz is the bandwidth of the spectral estimate] was specifically avoided in the analysis to minimize any effect due to LFP responses evoked by the monitor flicker.

Contrast response functions for the spike responses were well fit by hyperbolic sigmoid (Naka-Rushton) functions as expected (Albrecht and Hamilton 1982). The distribution of semi-saturation constants (c_{50}), exponent (n), and maximum response (R_{max}), were consistent with previous reports for V1 (Albrecht and Hamilton 1982). Hyperbolic sigmoid functions were also fit to the band-limited LFP contrast response functions (CRFs). However, these fits were poorly constrained, and the CRFs were often not well described by hyperbolic sigmoids, hence we decided to concentrate on the obvious qualitative aspects of CRFs rather than make an inappropriate quantitative comparison of the spike and LFP c_{50} and n distributions.

Spectral shape as temporal structure

The structure in the LFP spectrum induced by visual stimulation was quantified by the “shape” metric, SS. SS, was defined as

$$SS = R(f_{max})/\langle R \rangle_{15 < f < 240} \quad (4)$$

where $\langle R \rangle_{15 < f < 240}$ denotes the average R value estimated over all frequencies between 15 and 235 Hz, and f_{max} is the frequency within the gamma band where the largest R occurs. This metric provides a measure of the enhancement in the gamma-band power relative to the broadband (i.e., frequency nonspecific) enhancement in power. The maximum operation in choosing the peak was chosen because both the frequency of the gamma peak and the width were variable from site to site. Several other related metrics were employed with similar results. However, this one proved to be the most robust across sites and stimulus conditions, and it was also the most consistent with the spectral shape assessed “by eye.” Any deviation from a uniform distribution in a spectrum constitutes “temporal structure” in the time domain. The $1/f$ structure evident in the baseline LFP spectrum, indeed, corresponds to a significant temporal structure in the ongoing LFP possibly evidence of large-scale chaotic behavior (Freeman 2000). Likewise, any deviation from uniform enhancement of power constitutes a change in the temporal structure of the LFP. Here we concentrate specifically on the gamma band, which seems most prominent in the data. Note that we generally avoid the term oscillation in the context of the gamma-band-specific activity reported here in the LFP. Strictly speaking oscillations would be harmonic components that would manifest themselves as lines in the power spectrum rather than the broad peaks we observe, hence we prefer to discuss changes in the temporal structure (or spectral structure) in the response.

RESULTS

LFP power spectra are red, dominated by low temporal frequencies. The LFP fluctuates more and more quickly when a stimulus contrast is increased. Figure 1 shows an example “raw” data set of LFP and spikes recorded from a location in layer 2/3. Times of occurrence of spike discharge are displayed as a red tick overlying the black trace representing the LFP recorded simultaneously. One representative measurement of the LFP in response to each contrast is shown. Each trace contains 500 ms of LFP recorded before the stimulus was

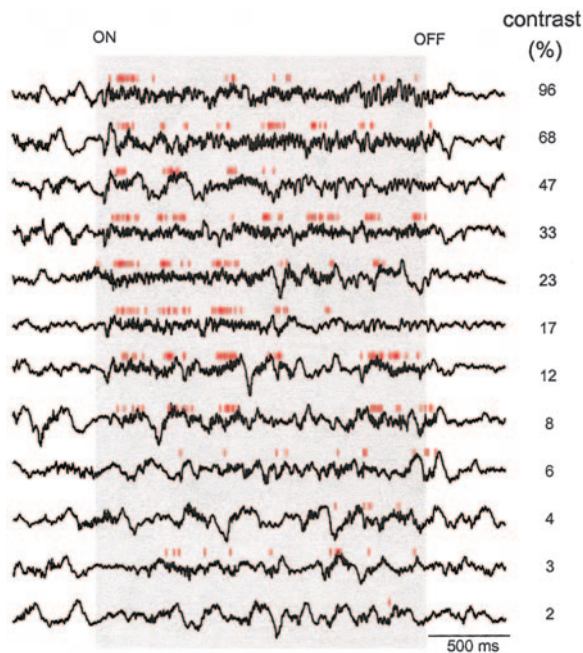


FIG. 1. Example local field potential (LFP) and spike records vs. contrast. LFP and spikes trains (red ticks) vs. contrast from an example site located in layer 2 + 3. These data represent 1 trial of 3 for each of the 12 contrasts which contributed to the spectral estimates used to quantify the response (shown in Fig. 7).

turned ON, and the stimulus drifted in this example for 2 s. Note that during the baseline (0% contrast) and low contrast periods, the LFP is dominated by the slow large-amplitude fluctuations, but at the high contrast, higher frequency fluctuations become more obvious. Spectral analysis of these raw data are presented in Fig. 7.

The most striking quality of the LFP power spectra measured in V1 (and apparently throughout cortex) (e.g., cf. Pesaran et al. 2002) is the immense dynamic range—more than three orders of magnitude—and fall-off of power at higher frequencies. An example LFP spectrum that is representative of the LFPs measured in V1 is shown in Fig. 2 from a second example recording site in layer 2/3. Power is plotted on a logarithmic scale for several levels of stimulus contrast between zero (baseline) and maximum (96% contrast). As described in METHODS, the stimulus was a drifting grating of optimum orientation, spatial frequency, temporal frequency, and the stimulus window was of optimum radius. Figure 2 illustrates the changes in the LFP power spectrum with increasing stimulus contrast. Within the gamma band, the 99% confidence intervals around the estimate of mean power are shown for the “high” contrast and baseline conditions. Note that due to a greater number of repeated measurements, the confidence limits in the baseline condition are very small. Also, the spectrum here in Fig. 2 (and also in Figs. 4 and 5) are only shown ≤ 200 Hz because the interesting aspects are concentrated at the lower frequencies. Indeed the spectra >200 Hz can generally be extrapolated from the spectra above ~ 150 Hz.

The LFP we measured in V1 is dominated by low-frequency components, and the amplitude spectrum of the 0% condition is roughly $1/f$ between 5 and 240 Hz. On top of the $1/f$ spectrum, the LFP power increases with stimulus contrast across most frequencies >25 Hz. There is very little relative

change with stimulus contrast in the LFP power in the low (<10 Hz)-frequency range despite the fact that these frequencies contain nearly all of the total power in the LFP. The largest relative changes are in the gamma frequency band, chosen somewhat arbitrarily, as discussed in METHODS, to lie between 25 and 90 Hz.

Frequency dependence of LFP CRF

The CRF of the LFP is steepest in a narrow band within the gamma frequency range. The relative sensitivity of the gamma band compared with the lower or higher frequencies is illustrated in Fig. 3A for the same example site as Fig. 2. The lower curve, representing the gamma band limited power in Fig. 3A, clearly has the steepest slope compared with either the middle curve, which represents the broadband (8–240 Hz) power in the LFP, or the upper curve, which represents the low-frequency (<10 Hz) power. Notably, the low-frequency power hardly changes with contrast and therefore has almost zero slope in Fig. 3A. A key observation about the LFP—that the low-frequency fluctuations in the LFP are huge compared with the higher-frequency components—is reiterated in Fig. 3A by the vertical offset on the logarithmic scale of the CRF for the low-frequency power and for the broadband power, relative to the gamma-band power. Also evident in Fig. 3A is the concentration of sensitivity to stimulus contrast in the gamma-band limited power, which despite being lower in total magnitude increases relatively much more with contrast than the broadband power or than the insensitive low-frequency band. Limiting the analysis to different bands from those defined here (e.g., high, 30–235 Hz) yields response gains intermediate between the gamma- and low- frequency curves. The definition of broadband power was chosen to be approximately the same as that used in the study of Logothetis et al. (2001) that previously linked stimulus contrast to the LFP activity.

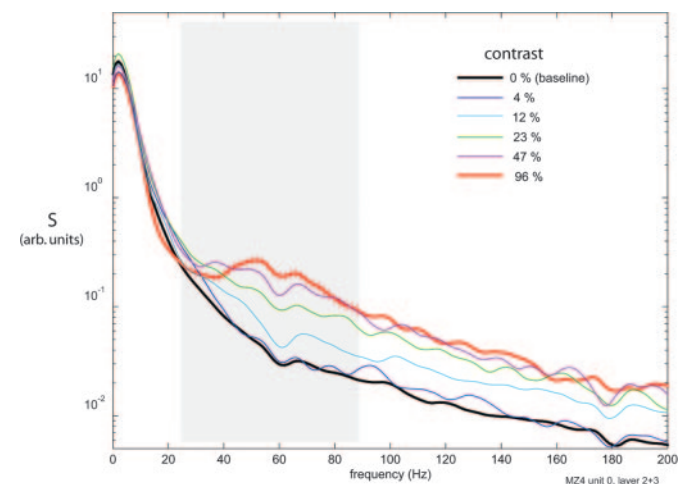


FIG. 2. Example LFP spectra for baseline (0%), intermediate, and high-contrast stimulation. Power spectrum of the LFP for a second representative recording site. The baseline (0% contrast) condition is shown in black, and the highest contrast (96%) is plotted in red. Four intermediate contrasts (4, 12, 23, and 47%) are shown as thin lines (blue, cyan, green, and magenta, respectively). The gray region represents the gamma- frequency band (25–90 Hz), and the error bars on the high-contrast spectrum (red) and baseline (black) represent bootstrapped 99% confidence intervals on the mean power for each frequency in this band.

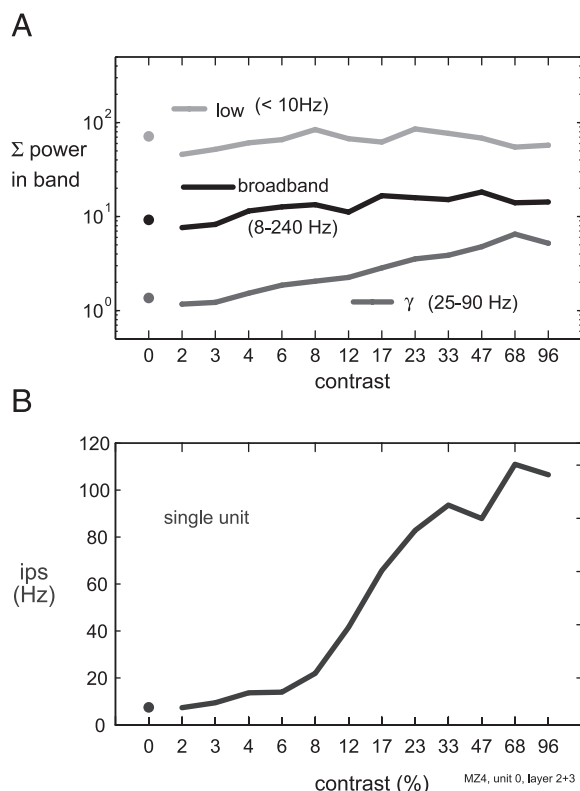


FIG. 3. Example contrast response functions for low-, broad-, and gamma-band-limited power, and spikes. *A*: contrast response functions for total band-limited power from the same example recording site as Fig. 2. The total (broadband) power was computed for each contrast by integrating the spectrum (e.g., Fig. 2) between 8 and 240 Hz and is plotted as a black line. The low frequency was derived from the sum over 0–10 Hz and the gamma-band power was computed by integrating power between 30 and 90 Hz. *B*: contrast response function for the spike rate response recorded simultaneously at the same site.

For comparison, the contrast-response function of the single-unit recorded at the same site is shown in Fig. 3*B*. The stimulus gratings were optimized in spatial and temporal parameters to elicit the maximal response from this neuron. The neuron's CRF is characteristic of V1 single units (e.g., Ohzawa et al. 1982); it increases over a relatively small range of stimulus contrasts above which the neuron's response saturates. The gamma-band LFP CRF for this site was among the most saturating among all the $n = 68$ recording sites.

Gamma-band "peak"

Although in many individual examples there is clearly a change induced in the gamma band by high contrast stimulation as evident in the LFP spectrum, the overall $1/f$ structure of the LFP spectra and huge dynamic range makes interpreting changes in the LFP activity somewhat difficult. For this reason, modulation spectra were derived by normalizing the power by the baseline level, frequency by frequency, as described in METHODS. By this construction the 0% contrast condition (baseline) is unity at all frequencies. Figure 4 shows a set of "modulation" spectra derived from the same LFP recording site as the example shown in Fig. 2. A gamma-band peak centered at around 60 Hz is obvious at the highest contrast. This gamma-band peak gradually emerges at high contrast. Indeed,

the peak is less evident at 47 than 96% contrast though both contrast levels lie within the simultaneously recorded neuron's "saturation" region (Fig. 3*B*). At lower contrasts, the modulation spectra in Fig. 4 are approximately flat in this example across all frequencies >40 Hz.

The peak that is evident in the LFP modulation spectrum at the highest contrast is evidence of a "temporal structure" (or "spectral structure") induced in the LFP by stimulation. To quantify this change in structure, a spectral shape metric, denoted SS, was computed. As described in METHODS, the SS measures the peak modulation of power in the gamma band normalized by the average enhancement in power from baseline across a 15- to 240-Hz band. At the lowest contrast for this example site the SS = 1.05, and the SS is increased at high contrast (Fig. 4, red line) to SS = 1.78.

Population average

The relationship between stimulus contrast and LFP activity, illustrated for one typical recording site in Figs. 2–4, generalizes across the population of $n = 68$ V1 sites for which we recorded contrast response functions. This generality is illustrated in the population average modulation spectrum versus contrast as shown in Fig. 5. For all frequencies above about ~ 30 Hz, the change in response power relative to baseline is $>100\%$. However, for the low-frequency band, the average modulation spectrum is nearly unchanged with contrast, confirming the insensitivity of low frequencies in the LFP to visual stimulation that we observed at the example site illustrated in Figs. 2–4. Although individual sites often contained relatively narrow (~ 25 Hz, such as the example in Fig. 4) peaks under high-contrast stimulation, these peaks were dispersed throughout the gamma band resulting in a relatively modest and broad, yet obvious, gamma band peak in the population average at the highest contrasts. The peaks at the four highest contrasts at 100 Hz reflect the ensemble activation locked to the stimulus monitor refresh (Williams et al. 2004) that was evident in many recordings. Likewise, the "dip" or "notch" around 60 Hz due to an imperfect line-noise removal is, as mentioned in METHODS, also evident in most recordings.

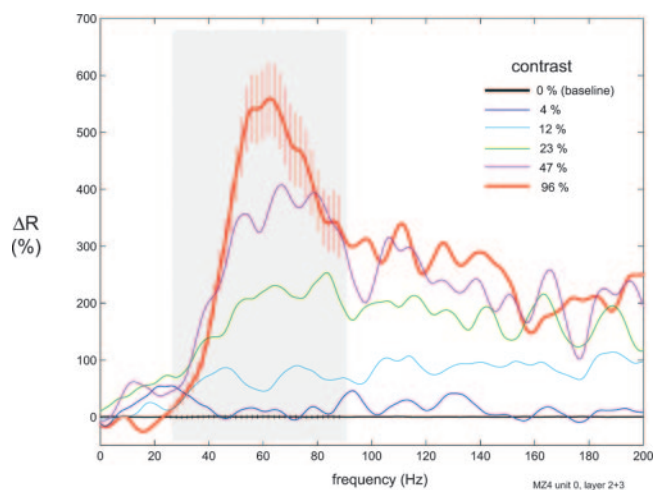


FIG. 4. Example modulation spectra at various contrasts. LFP modulation spectrum for the same example site as Figs. 2 and 3. Same conventions as Fig. 2. For each frequency, the estimate of power was normalized by the power estimated in the 0% contrast (baseline) condition.

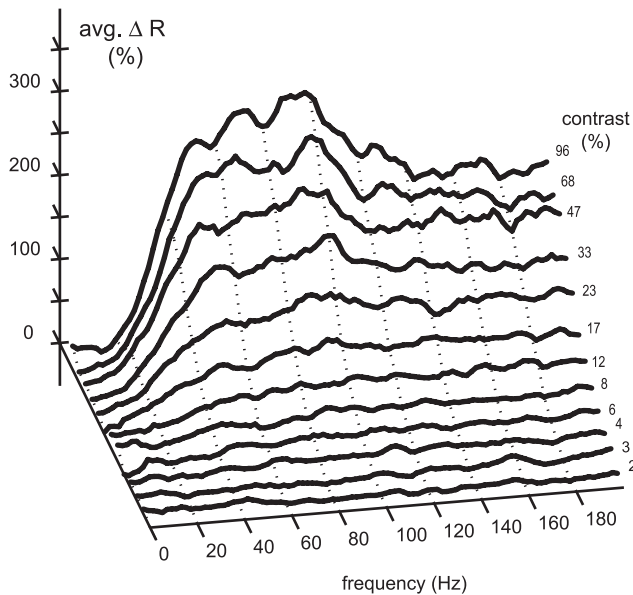


FIG. 5. Population average modulation spectra vs. contrast. Population average modulation spectrum vs. contrast over $n = 68$ recording sites for which complete contrast response functions were measured with otherwise optimal spatial stimuli.

The generality of the sensitivity to contrast of the gamma-band-limited LFP power, compared with the broadband or low-frequency power, is illustrated in Fig. 6. As in Fig. 3A, the power was integrated in each band (low, gamma, and broad) to produce contrast response functions for each site. The CRFs for each band were then normalized by their 0% contrast (baseline) level followed by averaging across the recording sites to produce the population averages shown. The results in Fig. 6 illustrate that in the population average, as in the earlier example site, the low-frequency band of the LFP does not modulate much with contrast but that the broadband modulates significantly ($\sim 90\%$) and the gamma band clearly modulates the most ($\sim 200\%$ from baseline).

For comparison, the average of normalized contrast-response functions for each of the single units recorded simultaneously with the LFPs is shown in Fig. 6C, labeled spikes. The average of the spike curves (upper curve) also illustrates the sigmoidal (or saturating) shape that is typical of individual V1 single-unit CRFs. In the same graph, a population average CRF for the gamma-band of the LFP is plotted. Both spikes and LFP are normalized for each site to range between 0 and 1. There is a rough similarity in the shape of the normalized average contrast-response functions for gamma-band LFP and neuron spikes. However, there is a small rightward shift of the gamma-band's contrast-response function.

Although the difference between the spike CRF and the gamma-band LFP CRF shown in Fig. 6C is subtle, the spectral shape, SS, clearly continues to increase through the highest contrasts. Figure 6B shows the population average spectral shape, SS, as a function of contrast. This SS CRF captures the gradual emergence of structure in the LFP—as evident in the power spectrum—as stimulus contrast increases. Across the population there is a relationship between contrast and SS (Kruskal-Wallis nonparametric ANOVA, $P < 10^{-15}$), where the SS is higher at the high contrast (mean SS = 1.54) than the low contrast (SS = 1.16).

Spike-LFP coherence

Even when the ensemble activity displays strong signatures of gamma-band temporal structures—as evident in a large LFP SS or a peaked spectrum—the spike trains remain largely unstructured. To illustrate this, in Fig. 7 both the LFP and spike trains for the example site shown in Fig. 1 are analyzed for temporal structure. Figure 7A shows the same raw data from Fig. 1 for the three repeats of the high (96%)-contrast stimulus. Figure 7B shows the modulation spectrum of the LFP for the data in Fig. 7A. The *inset* shows the power spectrum for these data as well as the baseline spectrum. Spectral analysis of the spike trains recorded at this example site shows two things. First, it shows that the signal to noise of the spectral estimates of spike trains is not as high as for the LFP as illustrated by the large confidence intervals around the high-contrast spike spectrum in Fig. 7D. Second, and most importantly, spectral analysis shows that the evidence for temporal structure in the gamma-band (i.e., deviation from the Poisson expectation) in the spike trains is weak as evident from the small and inconsistent deviations in the spike spectrum shown in Fig. 7D. If the absence of strong temporal structure observable in our spike trains is due simply to signal to noise, a temporal structure might be observable when compared with the LFP. The spectral coherence between the spikes and LFP measures how

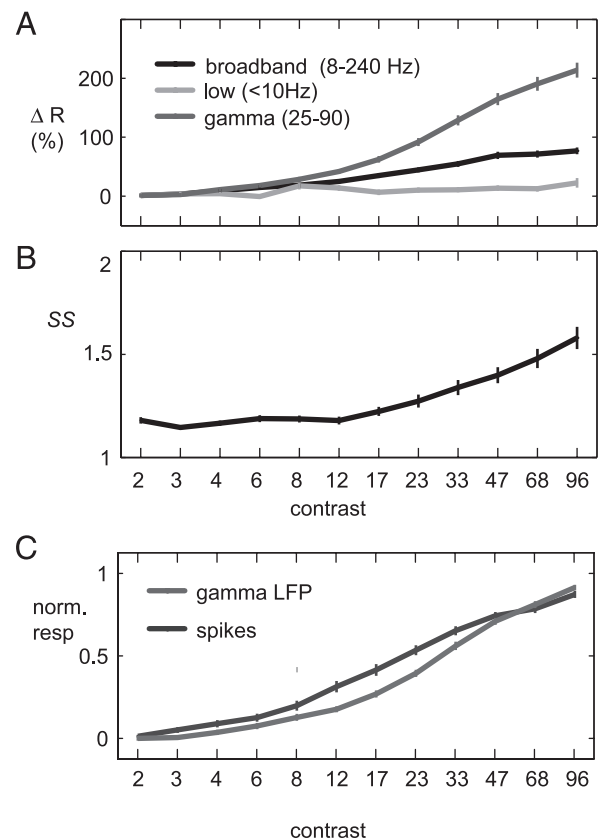


FIG. 6. Population average contrast response functions. A: population average of normalized contrast response functions (CRFs) for low-, broad-, and gamma-band-limited modulation in power with respect to baseline in the LFP. B: population average contrast gain for the spectral shape (SS) of the LFP. C: average rate-normalized CRF for the simultaneously recorded spike activity. Error bars on all CRFs (A–C) represent \pm SE over $n = 68$ recording sites.

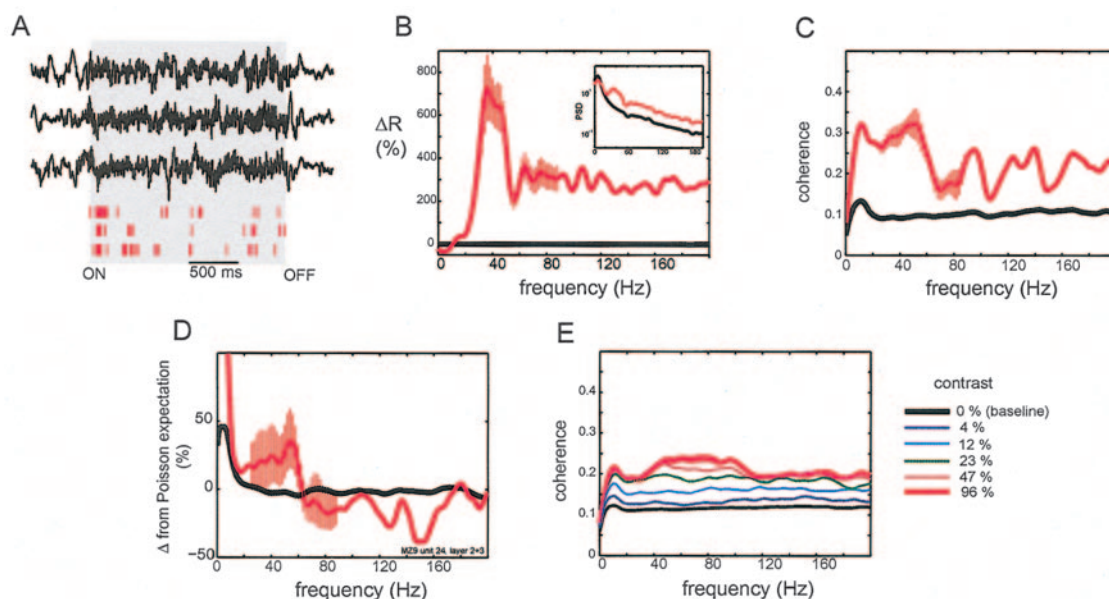


FIG. 7. LFP, spike, and LFP-spike coherence spectrum for a second example site. Population average LFP-spike coherence. *A*: example LFP and spikes for 3 repeats of the same high-contrast grating for the same example recording site shown in Fig. 1. *B*: LFP modulation spectrum (*inset*: LFP power spectrum) for the high-contrast recording at this site. *C*: spike-LFP coherence spectrum for the data shown in *A*. *D*: rate normalized spike power spectrum, plotted as percentage deviation from the rate expected from the Poisson expectation (see METHODS). *E*: population average LFP-spike coherence. Error bars represent \pm SE over $n = 68$ recording sites.

consistent the phase relationship between the two quantities are as a function of frequency. The coherence spectrum shown in Fig. 7C for the spike trains and LFP data in Fig. 7A indicate that there might be an excess of coherence in the gamma-band, although the magnitudes are weak. However, across all $n = 68$ recording sites the results were consistent as shown in Fig. 7E for several contrasts. At the highest contrast, in the population average there is a higher spike-LFP coherence in the gamma-band than other frequencies.

These LFP recordings were made in the course of ongoing single-unit studies that seek to correlate a unit's response properties with the lamina within V1 that its soma is located (e.g., Ringach et al. 2002; Sceniak et al. 2001). Hence, the laminar position of the recording electrode is known for the data set presented here. There were some weak trends regarding the manner in which the LFP spectra changed as stimulus strength was increased. Overall, there was a tendency for the superficial recording sites (layers 2 + 3) to have LFP spectra with larger gamma-band peaks than spectra from deeper recording sites. However, at the highest contrasts, sites where the LFP spectra had large SS values were found in all layers.

DISCUSSION

Major results

Increasing stimulus contrast caused the LFP to increase in amplitude and to become more structured, as indicated by the increase in spectral shape (SS index) at higher contrasts (Fig. 6B). The increase in spectral shape occurs over a contrast range within which the spike rates of cortical cells are saturating. This difference between the CRFs of SS (of the LFP) and spike rate suggests that the LFP and single-cell spike rate reflect two different aspects of cortical activity. This conclusion is also

powerfully supported by the large differences in response time course of the LFP and the spike rates of single cells that were reported previously (Logothetis et al. 2001). There is an increase caused by visual stimuli in both the variance of the ensemble activity, as Logothetis et al. (2001) reported, and in the temporal structure of the LFP such that the power becomes particularly concentrated in the gamma-band. The observation that this structure in the ensemble activity changed as overall level of activity increased has significant ramifications within the context of neuronal networks.

Comparison with previous results

In V1 cortex, previous studies have reported that some measure of LFP activity can be modulated by changes along a variety of stimulus dimensions. For instance, most studies have looked specifically (or implicitly) at the gamma band of the LFP, which has been shown to change with stimulus orientation in cats and monkeys (e.g., Gray and Singer 1989; Frien et al. 2000, respectively). Only recently has the LFP been characterized across a wide band in cat V1 (Kayser and König 2004; Siegel and König 2003), where it was reported that the most sensitive measure of stimulus selectivity for full field high-contrast gratings was gamma-band power. In monkey cortex, the gamma-band LFP activity was also shown to be more orientation selective than the signal at lower frequencies (Frien et al. 2000), but both bands were less selective for orientation than the spike activity due to a high level of activation for all stimuli. The only previous study in the literature that links the LFP activity to stimulus contrast correlated the total LFP variance, quantified as the root-mean-squared amplitude within 250 ms with the spatial contrast of a full-field checkerboard pattern in monkey V1 (Logothetis et al. 2001). From this study of Logothetis et al. (2001), it is unclear if the gamma-frequency-band power was differentially more

modulated than the higher- or lower-frequency components of the LFP at all contrasts or only at the highest contrast for which they performed the spectral analysis. Our work presented in this paper establishes that it is the gamma band of the LFP that is the most strongly modulated by visual input as evidenced by the steep slope of its contrast response function. Moreover, we report that the relative magnitude of modulation in the gamma-band surpasses the modulation across a broadband only for moderately high contrasts.

Generically, the LFP in cortex is dominated by low frequencies and has a roughly $1/f$ structure (e.g., Freeman 2000; Pesaran et al. 2002). However, in V1, previous studies of the LFP have not made this clear. Instead most V1 studies have either limited the analysis to a frequency range that did not extend much beyond gamma (i.e., below ~ 100 Hz) and/or have AC coupled the LFP (i.e., low-pass) signal at a relatively high frequency (i.e., above ~ 8 Hz) (e.g., Frien et al. 2000; Juergens et al. 1999; Kruse and Eckhorn 1996). This has left some readers to wonder if the LFP activation in the gamma frequency band was really especially modulated by visual input or simply a manifestation of band-pass filtering a broadband enhancement in power. In the most recent reports of LFP activity in visual cortex, the effective window of analysis has been widened (Gail et al. 2004; Kayser et al. 2003; Siegel and Konig 2003), but still the $1/f$ structure has been somewhat obscured by plotting power on a linear ordinate.

Predictions from theory

Temporally structured network activity in the form of oscillations is a hallmark of the steady-state dynamics of highly recurrent networks even when single units are firing irregularly (e.g., Brunel and Wang 2003; Kang et al. 2003; Wilson and Cowan 1972; and references therein). Therefore ensemble oscillations in V1 are expected under activated conditions, assuming V1 is dominated by recurrent activity especially inhibition. Furthermore, in quasi-realistic recurrent networks, the temporal structure evident in the ensemble as an oscillation emerges gradually as the overall level of activity in the network increases (Brunel and Wang 2003; C. Geisler, N. Brunel, and X. J. Wang, unpublished data), owing to the fact that the ensemble oscillation emerges as more and more of the units become coherent in their firing—that is, synchronized. In these theoretical treatments, the temporal structures discussed are bona fide oscillations in the sense that they are periodic and manifest a “line” in the activity power spectrum. However, in numerical network simulations patterns of temporal structure can be observed where the activity is less strictly periodic (e.g., “noisy” or “chaotic” oscillations) and the power spectrum of the population activity contains broad peaks rather than “lines” (e.g., Fig. 6e from Constantinidis and Wang 2004). These noisy temporal structures occur naturally and robustly for an array of synaptic parameters near the transition to stable periodic solutions (X. J. Wang, personal communication). Indeed, analysis of a numerical network model designed to mimic a variety of V1 single-unit response properties (Tao et al. 2004b) reveals a gamma-band-specific temporal structure in the aggregate ensemble activity (Tao et al. 2004a). In this numerical V1 network, the activity across an ensemble has a spectral peak located within the gamma band, whereas virtually all of the individual neurons have spike trains without

detectable temporal structure. This temporal structure in the ensemble activity is a consequence of the recurrent interaction between the neurons in the model. The population activity of the feed-forward model (i.e., recurrent interactions turned off) does not contain any gamma-band specific temporal structure.

We believe some of the specifics of the theoretical findings can be naturally applied to the results discussed here as follows. The frequency at which the temporal structure (oscillation) is concentrated would be expected from the theory to depend on the relative strengths and time constants of synaptic excitation and inhibition. For realistic neo-cortical values, the predicted oscillations would be expected to occur in the gamma-band (Brunel and Wang 2003; C. Geisler, N. Brunel, X. J. Wang, unpublished results). In Brunel and colleague’s analysis, the coherence of the population oscillation increases in strength as the feed-forward input to the circuit is increased or as the strength of recurrent interaction is increased. In V1, most single units increase their activity monotonically with stimulus contrast (e.g., Ohzawa et al. 1982) as does the afferent LGN input (e.g., Shapley and Enroth-Cugell 1984). Thus temporal structure in the V1 ensemble as measured in the LFP could be expected to emerge gradually with increasing stimulus strength.

What the LFP measures

An important issue to consider here is the LFP as a measure of neural activity. Because it is difficult, if not impossible, to implicate a precise physical source for the LFP it has perhaps been regarded as a “dirty” or substandard measure of neural activity, especially when compared with single-unit spike responses that have a clear physical source. Fortunately, there is circumstantial evidence that indicates that the LFP is closely related to the average activity within an appropriately local population. There is a very high correlation between simultaneously recorded intracellular voltage fluctuations and the LFP recorded nearby (McCormick et al. 2003; Penttonen et al. 1998; Steriade et al. 1996). Second, there is a strong rhythmic component to many, if not most, intracellular recordings when activated (e.g., Anderson et al. 2000; Azouz and Gray 2000; Bringuier et al. 1992, 1997; Gray and McCormick 1996; Jagadeesh et al. 1992; Volgushev et al. 2003), similar to what is observed in the LFP. On anatomical and theoretical grounds, it is believed that individual neurons are in under a constant synaptic barrage leaving them in a “high” conductance state (Rudolph and Destexhe 2003; Shadlen and Newsome 1998; Shelley et al. 2002), a consequence of which is that the membrane voltage is governed by an instantaneous function of the presynaptic population firing rate smoothed by the synaptic time constant. The two most obvious measures of aggregate population activity one could endeavor to make—directly recording the spike activity simultaneously from a large number of neurons or the indirect yet physically interpretable measurement derived from whole cell intracellular recordings—are technically prohibitive. Therefore it seems reasonable that we should be able to use the LFP to probe the activity of the local ensemble as we have done here.

Logothetis and his colleagues have demonstrated a link between the LFP and the signals measured noninvasively in the

brain by fMRI (reviewed in Logothetis and Wandell 2004). The blood-oxygen-level-dependent (BOLD) signal measured by the fMRI is predicted more strongly by the simultaneously recorded power in the LFP than in the spiking activity (Logothetis et al. 2001). They interpret the LFP and therefore the BOLD signal to be related to the activity of local processing (synaptic activity), whereas the spiking activity is related to the net "output" signal of the brain region, in this case V1, consistent with the belief that the BOLD signal is driven by the metabolic demand of the local population of neurons. Indeed, under a pharmacological manipulation that nearly abolishes the spiking activity, the LFP and BOLD signal remain largely unchanged (Logothetis 2003). This result starkly illustrates the disconnect between the spiking activities and the BOLD signal. The strong link between the LFP and the fMRI BOLD signal reinforces the notion that the LFP is a measure of aggregate neural activity.

As discussed in the preceding text, the LFP is not a simple sum over the spiking activity of nearby neurons or a population firing rate. Rather it is related to the total synaptic activity within the local network (Freeman 1975; Logothetis 2002). In V1 cortex, synaptic inhibition is thought to exert an especially strong influence in the mechanisms underlying single-unit response selectivities and dynamics (e.g., reviewed in Shapley et al. 2003) despite the fact that, anatomically, neurons expressing inhibitory neurotransmitter are relatively rare in V1 (i.e., 25% in Beaulieu et al. 1992). Strong inhibition is a hallmark of the theoretical and numerical neural networks discussed in the preceding text that can account for the temporal structure in the ensemble activity (Brunel and Wang 2003), the highly variable structure of single-unit spike trains (Rudolph and Destexhe 2003), and a variety of visual response properties of V1 neurons (Tao et al. 2004b). Therefore we conjecture that a disproportionate amount of the network activity captured in the LFP originates within inhibitory interneuron populations, compared with conventional single-unit recordings where, at best, interneurons are sampled according to their anatomical proportion (1/4–1/10) (Beaulieu et al. 1992). If the LFP does indeed depend on the activity of this important sub-class of neurons—inhibitory interneurons—it is doubly important because small, compact, inhibitory interneurons are critically under-sampled by single-unit recording techniques (Henze et al. 2000) that favor the large-amplitude spikes generated by larger, often pyramidal, neurons that happen to be excitatory. Very recently, preliminary evidence directly linking the LFP fluctuations specifically with inhibitory synaptic events in vivo has been reported for ferret cortex (Haider et al. 2004). This group also reported that the subthreshold synchronization between two neurons recorded in vivo in cat V1 was particularly more evident for inhibitory synaptic events than excitatory ones (Hasenstaub et al. 2004).

We have observed that the structure in the ensemble activity, as measured by the SS of the LFP spectra, increases steadily through the highest contrasts (e.g., Fig. 6B). However, at the highest levels of stimulus strengths used here, the LFP power (both broad and gamma band) begins to saturate (Fig. 6C), and at these contrasts, a majority of single units have already saturated in their response (e.g., Albrecht and Hamilton 1982). That is, for increases in

stimulus strength when the contrast is already high, V1 cortex changes not by increasing the total number of action potentials fired per unit time but by increasing the coherence among the neurons, resulting in a patterning of the activity in time. This is tantalizingly similar to effect of attention in monkey area V4 reported by Fries et al. (2001). They reported that rather than modulating the firing rate of neurons, engagement of attention increased the coherence between the recorded spikes and the LFP. Again, as we report here in V1, in the same recordings they did not find strong evidence for gamma-band structure in the spike trains.

Finally, something should be said regarding the behavioral relevance of these optimal stimuli, considering that oscillations and other temporal structures (e.g., coherence among multiple neuron's response) are often interpreted according to their utility in feature integration (e.g., Singer and Gray 1995). The findings here seem somewhat at odds with the notion that gamma-band oscillations signal something associated specifically with perception or the connectedness among the local parts of a perceived whole because the stimuli used here—patches of drifting grating—are so very simple. In fact, a recent paper by Gail et al. (2004) reveals that lower-frequency (<30 Hz) modulations in LFP power (and coherence) and not the gamma-band components correlate with the perception in the context of binocular rivalry. Instead, we interpret the structuring that emerges in the LFP recorded in V1 cortex—a gamma-band peak in the activity spectrum—as a natural consequence (i.e., expected theoretically) of the high levels of recurrent network activity recruited by stimulating the system with a high-contrast stimulus that is optimal for a single unit. In other words, observation of gamma-band-specific activity in the form of an oscillation (or peak in the spectrum) is indicative of a high level of activity within the network.

Although LFP recordings have long been used as measurable quantities of neural activity, the imprecision in which the source of the LFP can be defined has made them less attractive and, perhaps, less useful in understanding cortical function than spike activity. However, when they are recorded in addition to spike activity, the LFP activity can provide a context that is very useful in elucidating brain function.

ACKNOWLEDGMENTS

We thank M. Hawken, P. Williams, D. Xing, and S. Joshi for help with the experiments, and helpful comments about the manuscript. We also thank L. Tao, M. Shelley, and R. C. Reid for helpful discussions, and anonymous reviewers for insightful critique.

GRANTS

This research was supported by National Eye Institute Grants R01 EY-01472, R01 EY-08300, and T32 EY-07158.

REFERENCES

- Albrecht DG and Hamilton DB.** Striate cortex of monkey and cat: contrast response function. *J Neurophysiol* 48: 217–237, 1982.
- Anderson J, Lampl I, Reichova I, Carandini M, and Ferster D.** Stimulus dependence of two-state fluctuations of membrane potential in cat visual cortex. *Nat Neurosci* 3: 617–621, 2000.
- Azouz R and Gray CM.** Dynamic spike threshold reveals a mechanism for synaptic coincidence detection in cortical neurons in vivo. *Proc Natl Acad Sci USA* 97: 8110–8115, 2000.
- Beaulieu C, Kisvárdy Z, Somogyi P, Cynader M, and Cowey A.** Quantitative distribution of GABA-immunopositive and -immunonegative neurons

- and synapses in the monkey striate cortex (area 17). *Cereb Cortex* 2: 295–309, 1992.
- Borg-Graham LJ, Monier C, and Fregnac Y.** Visual input evokes transient and strong shunting inhibition in visual cortical neurons. *Nature* 393: 369–373, 1998.
- Bringuier V, Fregnac Y, Baranyi A, Debanne D, and Shulz DE.** Synaptic origin and stimulus dependency of neuronal oscillatory activity in the primary visual cortex of the cat. *J Physiol* 500: 751–774, 1997.
- Bringuier V, Fregnac Y, Debanne D, Shulz D, and Baranyi A.** Synaptic origin of rhythmic visually evoked activity in kitten area 17 neurons. *Neuroreport* 3: 1065–1068, 1992.
- Brunel N and Wang X.** What determines the frequency of fast network oscillations with irregular neural discharges? I. Synaptic dynamics and excitation-inhibition balance. *J Neurophysiol* 90: 415–430, 2003.
- Buzsáki G.** Large-scale recordings of neuronal ensembles. *Nat Neurosci* 7: 446–451, 2004.
- Constantinidis C and Wang XJ.** A neural circuit basis for spatial working memory. *Neuroscientist* 10: 553–565, 2004.
- Destexhe A.** Spike-and-wave oscillations based on the properties of GABAB receptors. *J Neurosci* 18: 9099–9111, 1998.
- Efron B and Tibshirani R.** Bootstrap methods for standard errors, confidence intervals, and other measures of statistical accuracy. *Stat Sci* 1: 54–77, 1986.
- Ferster D and Miller KD.** Neural mechanisms of orientation selectivity in the visual cortex. *Annu Rev Neurosci* 23: 441–471, 2000.
- Freeman WJ.** Mesoscopic neurodynamics: from neuron to brain. *J Physiol Paris* 94: 303–322, 2000.
- Freeman W.** *Mass Action in the Nervous System*. New York: Academic, 1975.
- Friedman-Hill S, Maldonado PE, and Gray CM.** Dynamics of striate cortical activity in the alert macaque: I. Incidence and stimulus-dependence of gamma-band neuronal oscillations. *Cereb Cortex* 10: 1105–1116, 2000.
- Frien A, Eckhorn R, Bauer R, Woelbern T, and Gabriel A.** Fast oscillations display sharper orientation tuning than slower components of the same recordings in striate cortex of the awake monkey. *Eur J Neurosci* 12: 1453–1465, 2000.
- Fries P, Reynolds JH, Rorie AE, and Desimone R.** Modulation of oscillatory neuronal synchronization by selective visual attention. *Science* 291: 1560–1563, 2001.
- Gail A, Brinkmeyer HJ, and Eckhorn R.** Perception-related modulations of local field potential power and coherence in primary visual cortex of awake monkey during binocular rivalry. *Cereb Cortex* 14: 300–313, 2004.
- Gray CM and McCormick DA.** Chattering cells: superficial pyramidal neurons contributing to the generation of synchronous oscillations in the visual cortex. *Science* 274: 109–113, 1996.
- Gray CM and Singer W.** Stimulus-specific neuronal oscillations in orientation columns of cat visual cortex. *Proc Natl Acad Sci USA* 86: 1698–1702, 1989.
- Haider B, Hasenstaub A, Duque A, and McCormick D.** Local recurrent excitation and inhibition in vivo are proportional and well balanced. *Soc Neurosci Abstr* 775.7, 2004.
- Hasenstaub A, Haider B, Duque A, and McCormick D.** Control of neuronal sensory responsiveness and spike timing by local recurrent activity. *Soc Neurosci Abstr* 985.15, 2004.
- Hawken MJ, Parker AJ, and Lund JS.** Laminar organization and contrast sensitivity of direction-selective cells in the striate cortex of the Old World monkey. *J Neurosci* 8: 3541–3548, 1988.
- Hawken MJ, Shapley RM, and Grosof DH.** Temporal-frequency selectivity in monkey visual cortex. *Vis Neurosci* 13: 477–492, 1996.
- Henze DA, Borhegyi Z, Csicsvari J, Mamiya A, Harris KD, and Buzsáki G.** Intracellular features predicted by extracellular recordings in the hippocampus in vivo. *J Neurophysiol* 84: 390–400, 2000.
- Hirsch JA, Alonso JM, Reid RC, and Martinez LM.** Synaptic integration in striate cortical simple cells. *J Neurosci* 18: 9517–9528, 1998.
- Holt GR, Softky WR, Koch C, and Douglas RJ.** Comparison of discharge variability in vitro and in vivo in cat visual cortex neurons. *J Neurophysiol* 75: 1806–1814, 1996.
- Hubel D and Wiesel T.** Receptive fields, binocular interaction, and functional architecture in the cat's visual cortex. *J Physiol* 160: 106–154, 1962.
- Jagadeesh B, Gray CM, and Ferster D.** Visually evoked oscillations of membrane potential in cells of cat visual cortex. *Science* 257: 552–554, 1992.
- Jarvis MR and Mitra PP.** Sampling properties of the spectrum and coherency of sequences of action potentials. *Neural Comput* 13: 717–749, 2001.
- Juergens E, Guettler A, and Eckhorn R.** Visual stimulation elicits locked and induced gamma oscillations in monkey intracortical- and EEG-potentials but not in human EEG. *Exp Brain Res* 129: 247–259, 1999.
- Kang K, Shelley M, and Sompolinsky H.** Mexican hats and pinwheels in visual cortex. *Proc Natl Acad Sci USA* 100: 2848–2853, 2003.
- Kayser C and Konig P.** Stimulus locking and feature selectivity prevail in complementary frequency ranges of V1 local field potentials. *Eur J Neurosci* 19: 485–489, 2004.
- Kayser C, Salazar RF, and Konig P.** Responses to natural scenes in cat V1. *J Neurophysiol* 90: 1910–1920, 2003.
- Kruse W and Eckhorn R.** Inhibition of sustained gamma oscillations (35–80 Hz) by fast transient responses in cat visual cortex. *Proc Natl Acad Sci USA* 93: 6112–6117, 1996.
- Logothetis NK.** The neural basis of the blood-oxygen-level-dependent functional magnetic resonance imaging signal. *Philos Trans R Soc Lond B Biol Sci* 357: 1003–1037, 2002.
- Logothetis NK.** MR imaging in the non-human primate: studies of function and of dynamic connectivity. *Curr Opin Neurobiol* 13: 630–642, 2003.
- Logothetis NK, Pauls J, Augath M, Trinath T and Oeltermann A.** Neurophysiological investigation of the basis of the fMRI signal. *Nature* 412: 150–157, 2001.
- Logothetis NK and Wandell B.** Interpreting the BOLD signal. *Annu Rev Physiol* 66: 735–769, 2004.
- McCormick DA, Shu Y, Hasenstaub A, Sanchez-Vives M, Badoual M, and Bal T.** Persistent cortical activity: mechanisms of generation and effects on neuronal excitability. *Cereb Cortex* 13: 1219–1231, 2003.
- Merrill EG and Ainsworth A.** Glass-coated platinum-plated tungsten micro-electrodes. *Med Biol Eng* 10: 662–672, 1972.
- Mitra PP and Pesaran B.** Analysis of dynamic brain imaging data. *Biophys J* 76: 691–708, 1999.
- Mitzdorf U.** Current source-density method and application in cat cerebral cortex: investigation of evoked potentials and EEG phenomena. *Physiol Rev* 65: 37–100, 1985.
- Nicholson C and Freeman JA.** Theory of current source-density analysis and determination of conductivity tensor for anuran cerebellum. *J Neurophysiol* 38: 356–368, 1975.
- Ohzawa I, Sclar G, and Freeman RD.** Contrast gain control in the cat visual cortex. *Nature* 298: 266–268, 1982.
- Penttonen M, Kamondi A, Acsády L, and Buzsáki G.** Gamma frequency oscillation in the hippocampus of the rat: intracellular analysis in vivo. *Eur J Neurosci* 10: 718–728, 1998.
- Percival D and Walden A.** *Spectral Analysis for Physical Applications: Multitaper and Conventional Univariate Techniques*. Cambridge, UK: Cambridge Univ. Press, 1993.
- Pesaran B, Pezaris JS, Sahani M, Mitra PP, and Andersen RA.** Temporal structure in neuronal activity during working memory in macaque parietal cortex. *Nat Neurosci* 5: 805–811, 2002.
- Ringach DL, Hawken MJ, and Shapley R.** Dynamics of orientation tuning in macaque primary visual cortex. *Nature* 387: 281–284, 1997.
- Ringach DL, Shapley RM, and Hawken MJ.** Orientation selectivity in macaque V1: diversity and laminar dependence. *J Neurosci* 22: 5639–5651, 2002.
- Rudolph M and Destexhe A.** The discharge variability of neocortical neurons during high-conductance states. *Neuroscience* 119: 855–873, 2003.
- Sceniak MP, Hawken MJ, and Shapley R.** Visual spatial characterization of macaque V1 neurons. *J Neurophysiol* 85: 1873–1887, 2001.
- Shadlen MN and Newsome WT.** The variable discharge of cortical neurons: implications for connectivity, computation, and information coding. *J Neurosci* 18: 3870–3896, 1998.
- Shapley R and Enroth-Cugell C.** Visual adaptation and retinal gain controls. In: *Progress in Retinal Research*, edited by Osborne N and Chader G. New York: Pergamon, 1984, vol. 3, chapt. 9, p. 263–346.
- Shapley R, Hawken M, and Ringach DL.** Dynamics of orientation selectivity in the primary visual cortex and the importance of cortical inhibition. *Neuron* 38: 689–699, 2003.
- Shelley M, McLaughlin D, Shapley R, and Wiesel J.** States of high conductance in a large-scale model of the visual cortex. *J Comput Neurosci* 13: 93–109, 2002.
- Siegel M and Konig P.** A functional gamma-band defined by stimulus-dependent synchronization in area 18 of awake behaving cats. *J Neurosci* 23: 4251–4260, 2003.

- Singer W and Gray CM.** Visual feature integration and the temporal correlation hypothesis. *Annu Rev Neurosci* 18: 555–586, 1995.
- Softky WR and Koch C.** The highly irregular firing of cortical cells is inconsistent with temporal integration of random EPSPs. *J Neurosci* 13: 334–350, 1993.
- Steriade M, Amzica F, and Contreras D.** Synchronization of fast (30–40 Hz) spontaneous cortical rhythms during brain activation. *J Neurosci* 16: 392–417, 1996.
- Tao L, Henrie A, Shelley M, and Shapley R.** Ensemble activity in a neuronal network of macaque primary visual cortex. *Soc Neurosci Abstr* 648.18, 2004a.
- Tao L, Shelley M, McLaughlin D, and Shapley R.** An egalitarian network model for the emergence of simple and complex cells in visual cortex. *Proc Natl Acad Sci USA* 101: 366–371, 2004b.
- Thomson D.** Spectrum estimation and harmonic analysis. *Proc IEEE* 70: 1055–1096, 1982.
- Thomson D and Chave A.** Jackknifed error estimates for spectra, coherences, and transfer functions. In: *Advances in Spectrum Analysis and Array Processing*, edited by Haykin S. Englewood Cliffs, NJ: Prentice-Hall, 1991, vol. 1, chapt. 2, p. 58–113.
- Volgushev M, Pernberg J, and Eysel UT.** Gamma-frequency fluctuations of the membrane potential and response selectivity in visual cortical neurons. *Eur J Neurosci* 17: 1768–1776, 2003.
- Williams P, Mechler F, Gordon J, Shapley R, and Hawken M.** Entrainment to video displays in primary visual cortex of macaque and humans. *J Neurosci* 24: 8278–8288, 2004.
- Wilson HR and Cowan JD.** Excitatory and inhibitory interactions in localized populations of model neurons. *Biophys J* 12: 1–24, 1972.
- Xing D, Ringach DL, Shapley R, and Hawken MJ.** Correlation of local and global orientation and spatial frequency tuning in macaque V1. *J Physiol* 557: 923–933, 2004.